# Elucidating the Molecular Basis of pH Activation of an Engineered Mechanosensitive Channel

Kalyan Immadisetty, Adithya Polasa, Reid Shelton, and Mahmoud Moradi*

*Department of Chemistry and Biochemistry, University of Arkansas, Fayetteville, AR 72701*

E-mail: moradi@uark.edu

**Abstract**

Mechanosensitive (MS) channels detect and respond to changes in the pressure profile of cellular membranes and transduce the mechanical energy into electrical and/or chemical signals. By re-engineering, however, the activation of some MS channels can be triggered by chemical signals such as pH change. Here, for the first time, we have elucidated, at an atomic level, the activation mechanism of an engineered MscL channel in response to the pH changes of the environment through a combination of equilibrium and non-equilibrium molecular dynamics (MD) simulations. The key highlights of our proposed activation mechanism are that: (1) periplasmic loops play a key role in activation, (2) loss of various hydrogen bonding and salt bridge interactions in the engineered MscL channel causes the opening of the channel, and (3) the most significant interactions lost during the activation process are those between the transmembrane (TM) helices 1 and 2 (TM1 and TM2). The orientation-based method in this work for generating and optimizing an open model of engineered MscL is a promising method for generating unknown states of proteins and for studying the activation processes in ion channels. This work facilitates the studies aimed at designing pH-triggered drug delivery liposomes (DDL), which embed MscL as a nanovalve.

**Keywords:** MscL channel, activation mechanism, un-biased MD simulations, non-equilibrium MD simulations

# Introduction

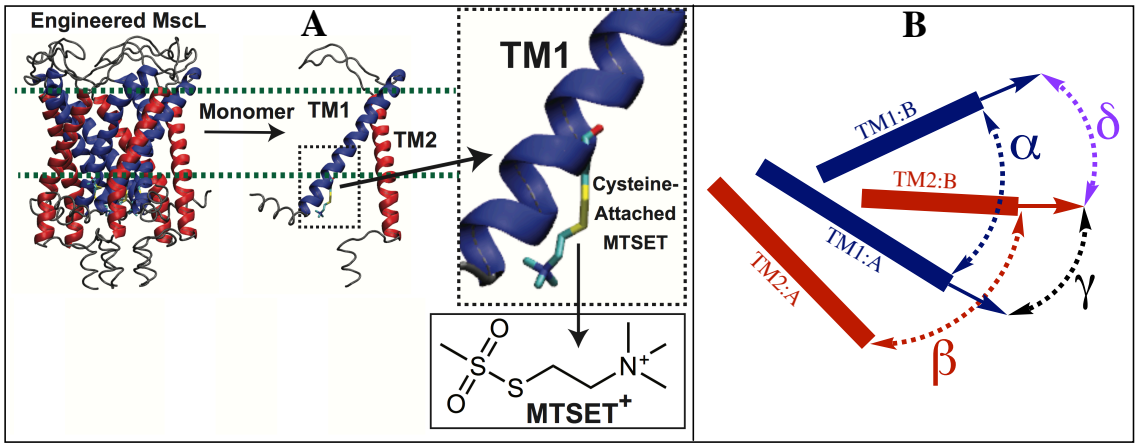


**Fig. 1.** Engineered MscL channel and different orientation angles calculated. (A) pH-sensitive labels attached to G22C ecMscL (A20C tbMscL) mutant enable a pH-dependent activation mechanism for MscL channel. MTSET+ (bottom right panel) attachment activates MscL even in physiological conditions. (B) $\alpha$ is the angle between TM1s of neighboring domains, $\beta$ is the angle between TM2s of the neighboring domains, $\gamma$ is the angle between TM1 and TM2 of the neighboring domains, and $\delta$ is the angle between TM1 and TM2 of same domain.

Mechanosensitive Channel of Large Conductance (MscL) is a ∼80-kDa homo-pentameric membrane protein with each subunit consisting of two $\alpha$-helical transmembrane (TM) helices (Fig. 1) .[1,2] MscL channels detect and respond to changes in the pressure profile of cellular membranes and transduce the mechanical energy into electrical and/or chemical signals.[3–6] However, by re-engineering, the activation of MscL can be triggered by chemical signals such as pH change,[7–14] which is a basis for using an engineered MscL as a pH-sensing nanovalve in a drug delivery liposome (DDL).[2,8,15]

While many molecular dynamics (MD) studies have been conducted to study the MscL activation, the techniques used in these studies were based on simplifications such as coarse-graining[16–18] or inducing the transition by applying large forces.[19–23] Other computational approaches such as simple (static) modeling[24] and continuum models[25–27] have been used

for the study of MscL activation as well. Here, for the first time we attempted to study the mechanism of activation of engineered MscL by pH changes at an atomic level nd within the thermodynamic conditions, so that the information can be used to develop better nanovalves. In this work we conducted all-atom equilibrium un-biased MD simulations followed by non-equilibrium simulations, in which relatively small forces (as compared to previous studies) were applied to impose rotational changes using the orientation quaternion technique.[28–32]

In the un-biased equilibrium MD simulations initially performed we observed that the introduction of labels partially opened the channel, especially near the narrowest region that is present on the intracellular side. However, the channel did not open completely on the extracellular side. To see the maximum extent to which the channel opens, we performed non-equilibrium simulations, in which the experimentally derived MscL structure (SMFRET) was used as a reference structure to open the channel. Further, we relaxed the open state structures of the channel resulting from non-equilibrium simulations via un-biased equilibrium simulations to see if the structures are stable in open state. The non-equilibrium wild-type (WT) structure collapsed back to the closed conformation, while the engineered structure remained open, even though it is closed compared to the engineered structure resulting from the non-equilibrium simulations. Finally, we propose a mechanism for the activation of the channel and is discussed in detail in the following results and discussion section.

# Methods

Crystal structure of MscL in closed (in-active) state (PDB: 2OAR)[33] was downloaded from pdb.org. Initially the system was prepared using the Molecular Operating Environment (MOE) software[34] by removing the crystal waters, assigning the appropriate protonation states for the residues using protonate3D facility and also by adding hydrogens and other missing atoms. Further, CHARMM-GUI web-server[35,36] was used to place the protein in the 1-palmitoyl-2-oleoyl-sn-glycero-3-phosphocholine (POPC) membrane bilayer and also to solvate and build the system. 0.15 mM NaCl was added and the system has 181 sodium and 181 chloride ions. Overall, the total size of the system was $\approx 150\times150\times130\,\text{Å}^3$. The total number of lipids were 603 (298 lipids in the upper leaflet and 305 lipids in the lower leaflet) and TIP3P[37] waters were 60,027. The total number of atoms in the system were approximately 270,524. NAMD2.10/2.113[38] was used to simulate the system in periodic boundary conditions in the NPT ensemble at 310 K using a Langevin integrator with a damping coefficient of $\gamma = 0.5\,\text{ps}^{-1}$ and 1 atm pressure was maintained using the Nosé-Hoover Langevin piston method.[39,40] Time step used was 1 fs and the system was equilibrated for 1000 ns. Trajectory was saved every 40 ps. CHARMM36 all-atom additive force field parameters were used to simulate the entire system .[41,42] We also prepared a second system by mutating A20 to cysteine in each subunit of MscL. Next, a pH-sensing label MTSET+ was attached to each mutated residue (total 5 labels). Further, the system was prepared using the procedure explained above. The size of the system and the total number of atoms were approximately similar to the above, except that this system has extra labels attached to the cysteines at position 20. CHARMM General Force Field (CGenFF) parameters was used for the MTSET+ labels. A third system was also prepared to serve as a control. In this system, A20 in only one subunit was mutated to cysteine and pH-sensing label MTSET+ was attached. System was prepared using the similar protocol explained above. Systems 2 and 3 were simulated each for 1000ns respectively. We also performed two extra simulations (sets 2 &

3) for each of the above three systems. The two extra simulations were restarted from the first simulations by using the configurations at 150ns and 200ns as the input in all three cases. Since the labels attached to monomers 2 & 4 in 5-MTSET were oriented differently from the other 3, we manually re-oriented them similar to the other 3 and we call this 5-MTSET(A)(Fig. S1). Prior to equilibration, we first energy minimized each parent system (Set1) for 10,000 steps via. conjugate gradient algorithm.[43] Further, we relaxed the parent systems via. a multi-step restraining simulations totaling $\sim$1 ns,[35] which were performed in an NVT ensemble. The non-bonded interactions were cutoff at $10-12$ Å and the long-range electrostatic interactions were computed with particle mesh Ewald (PME) method.[44] One data point for 1 ns was collected for the statistical analysis. Trajectories were visualized using VMD.[45] Principle component analysis (PCA) was carried using PRODY software[46] on a ensemble of dcd structures and 20 modes were generated. Only C$\alpha$ atoms were considered for the PCA calculations. The details of the methodology can be found else where.[47,48] Hydrogen bond and salt bridge interaction analysis was conducted via VMD plugins. The cut-off distance and angle were 3.5 Å and 30° respectively, for the hydrogen bond analysis. Only one hydrogen bond for an interaction pair was counted. For salt bridge analysis, the cut-off distance was 4 Åand the distance between the oxygen atoms of the acidic residues and nitrogens of basic residues was calculated.

In the non-equilibrium simulations, we opened equilibrated WT, 5-MTSET and 5-MTSET(A) structures in an 100ns simulation each using orientation colvars. We have used small molecule FRET (SM-FRET) based open state model of Mscl as a target for the non-equilibrium simulations. Each simulation was repeated one more time and the force constant used was 10,000 $kcal/mol.rad^2$ (Table 2).

**Table 1: Equilibrium MD simulations.**

| | **WT** | **5-MTSET** | **1-MTSET** | **5-MTSET(*)** |
|---|---|---|---|---|
| Set-1 | 1000ns | 1000ns | 1000ns | 500ns |
| Set-2 | 500ns | 500ns | 500ns | |
| Set-3 | 500ns | 500ns | 500ns | |

**Table 2: Protocol for non-equilibrium and the follow up equilibrium simulations.**

| **Step** | **Force Constant (k)** ($kcal/mol.rad^2$) | **Time** ($ns$) |
|---|---|---|
| 1 | 10,000 | 100 |
| 2 | 10,000 | 5 |
| 3 | 10,000 to 1000 | 5 |
| 4 | 1000 to 0 | 10 |
| 5 | 0 | 240 |

# Results and Discussion

## Equilibrium Simulations

### Protein response to the engineered labels is spontaneous

First to see if the systems stabilized we calculated the protein $C_\alpha$ RMSD (Fig. 2). RMSD of the WT (all 3 sets) stabilized approximately at 5 Å (Fig. 2A). In the case of 1-MTSET and 5-MTSET, RMSDs spontaneously went up (with in first 100ns) and were stabilized after 200ns and spread between 6-8 Å (Fig. 2B) for 5-MTSET, where as in the case of 1-MTSET, sets 1 & 3 were stabilized approximately at 6 Å after 200ns and set 2 went upto 7.5 Å and not stabilized yet (Fig. 2C). This highlights the fact that the impact of labels is spontaneous and opened the channel instantly. Also, this establishes that even one label created enough disturbance in the protein environment, however, disturbance is greater when there are 5 labels than one. RMSD of the entire protein follows the same pattern as RMSD of extracellular loops (Figs. S3 A, B and C), highlighting the fact that the loops are driving or dominating the changes in the protein. This is quiet interesting keeping in mind the fact that although labels are attached at the intracellular side, the immediate impact is seen not just on the intracellular side, but also on the extracellular side, which is evidanced by the immediate rise in RMSD of the loops.

### Impact of labels is symmetrical

To see the impact of labels on the specific regions of the protein we measured the root mean square fluctuation (RMSF). Irrespective of the system, extracellular loops are dominating compared to the rest of the protein, although, the extent of fluctuation varies between the systems. RMSF of the entire protein in the case of WT is between 0.5-6 Å (Fig. S2A), for 1-MTSET 0.5-7 Å except for first sub-unit 1 (S1), where it is fluctuating between 0.5-11 Å (Fig. S2B). For the 5-MTSET, the RMSF of all sub-units are evenly fluctuating between

0.5-7 Å except for sub-unit 2 (S2), where it went upto 9.5 Å (Fig. S2C). RMSF of TM helices in WT are varying between 0.5-2 Å (Fig. S2D), where as in 1-MTSET between 0.7-3 Å (Figs. S2E), and in other cases between 1.0-3.5 Å (Figs. S2F). This shows that the impact of the labels in the 5-MTSET systems is symmetrical on the TM helices, although it varies in the extracellular loops.

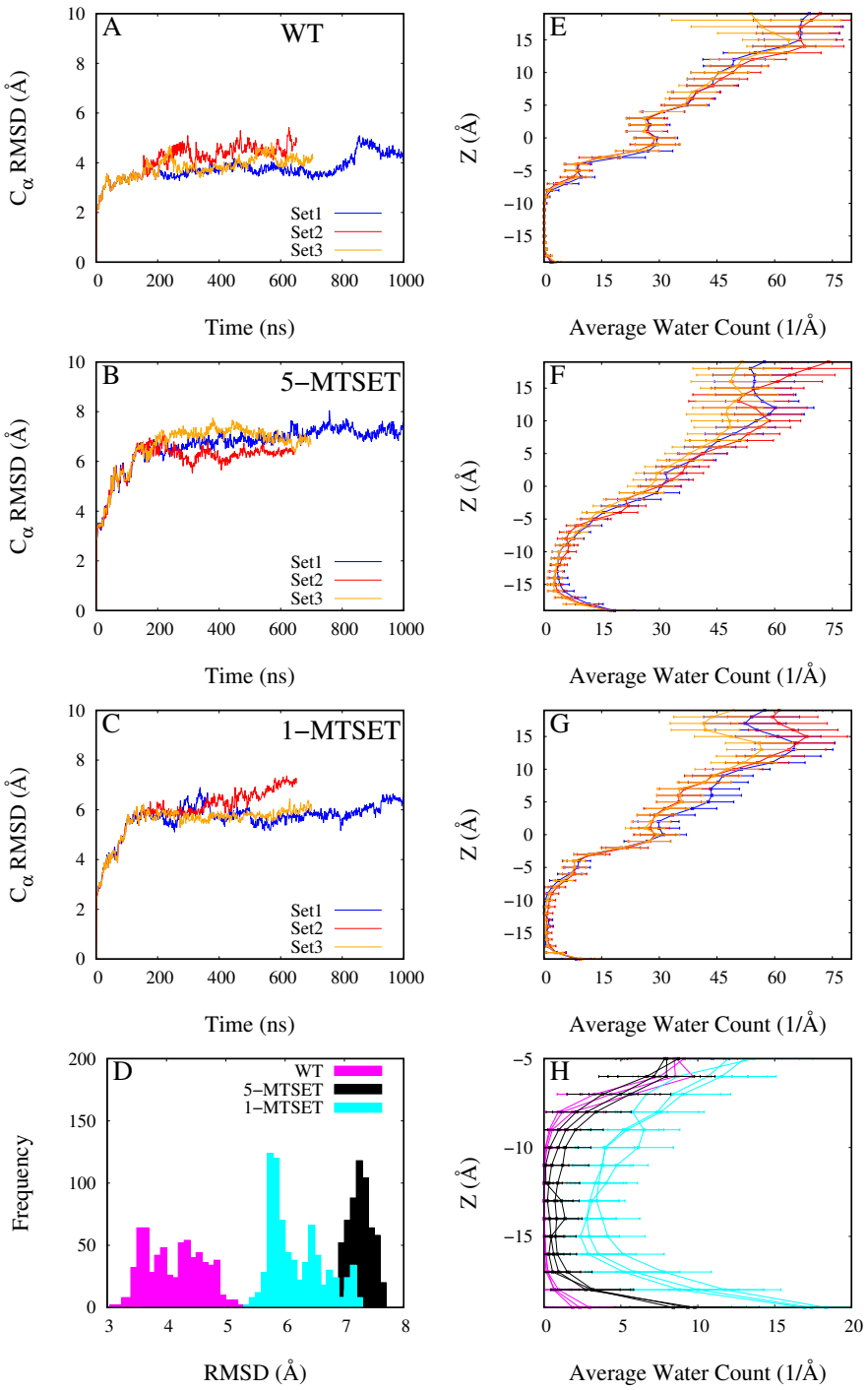


**Fig. 2.** Protein RMSD ($C_\alpha$) and water count across the channel pore. (A-C) WT (A) RMSD was stablized around 4 Å and the 5-MTSET (B) were distributed between 6-8 Å, while the 1-MTSET was stabillized around 6 Å, except the set-2 simulation (C). (D) Frequency distribution of these RMSD's were shown in D. Only the last 300ns of the trajectory was considered for generating the frequency plot. Z between -9 and -19 Å reflects the narrower region of the channel that restricts the passage of the ligands across the channel.

**Labels opened the channel partially and 5-MTSET is more efficient than the 1-MTSET**

To estimate the extent of opening of the channel, the water content across the pore was calculated. We observed that the WT is completely closed and there is no water across the pore (Z = -9 to -20 Å, Fig. 2E), and in the case of 1-MTSET, single label failed to open the channel, although there is some water in the narrower part of the channel occasionally (Fig. 2G). In the case of 5-MTSET (sets 1, 2 and 3), the channel is more open compared to the WT and 1-MTSET (Figs. 2 F, H). Overall the extent of the opening of the channel, particularly near the narrow region is as follows 5-MTSET > 1-MTSET > WT (Fig. 2H). However, this trend is reversed near the extracellular loop region (Z = 15-20 Å), and the trend is WT > 5-MTSET > 1-MTSET (when compared the average of set-1 simulations, Figs. 2 E, F, G). We believe this is due to the collapse of the extracellular loops into the center of the channel pore in the case of the 1-MTSET and 5-MTSET and blocking the channel pore on the extracellular side, which do not happen in the WT (Figs. S3 C, D, E, and F). Overall, based on our water content analysis we conclude that 5-MTSET is more effective than the 1-MTSET in opening the channel, hence, we will not consider 1-MTSET for further analysis in the rest of the paper.

**Labels distort the hydrogen bond interaction network in the MscL**

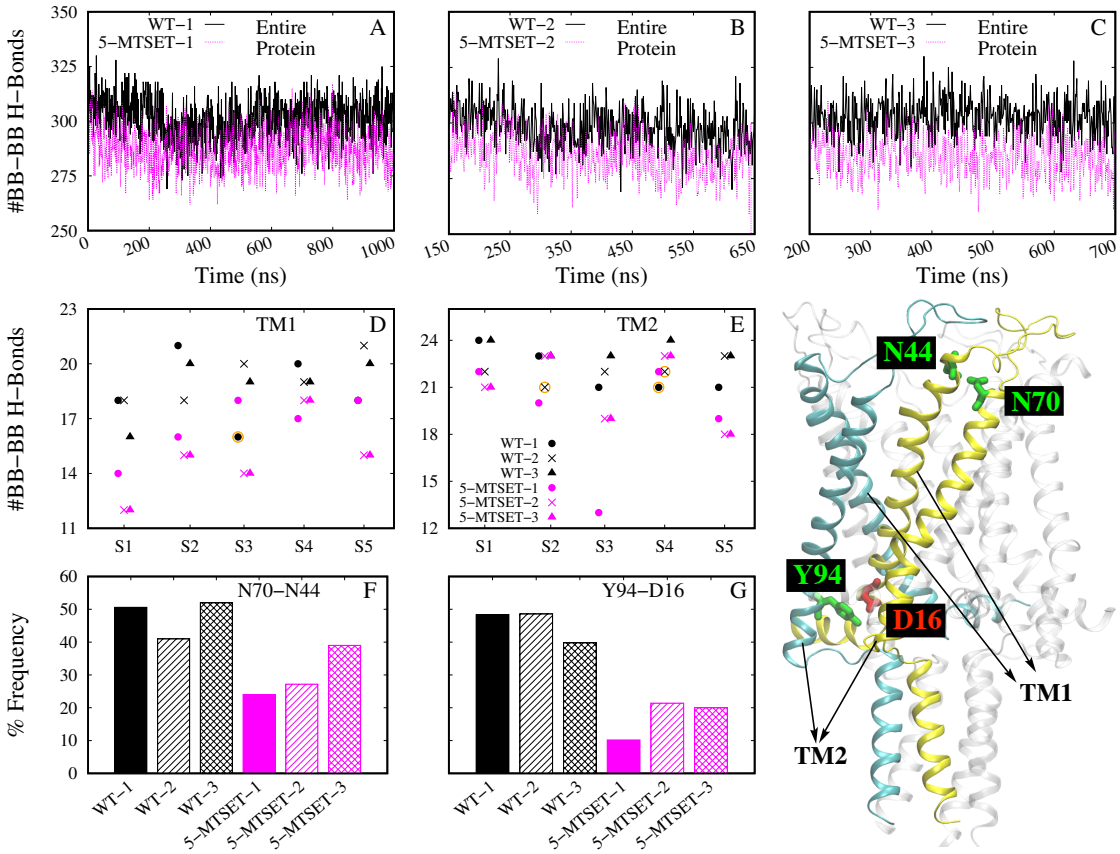


**Fig. 3.** WT vs. 5-MTSET hydrogen bond interaction analysis. (A-C) Comparison of the BB-BB hydrogen bonds of three trials of WT and 5-MTSET respectively. (D-E) BB-BB hydrogen bonds (with $> 70\%$ interaction frequency) of TM1 and TM2 of all monomers of WT and 5-MTSET respectively. (F-G) SC-SC interaction frequencies (average of all 5 monomers) of N70-N44 and D16-Y94 in WT and 5-MTSET respectively. D16-Y94 and N44-N70 hydrogen bond interaction pairs are showed in H. D16 (TM1, i) - Y94 (TM2, i+4) interaction pair was on the intracellular side near the labels forming between the TM1 and TM2 of neighboring monomers (i-i+4). N44 (TM1, i) - N70 (TM2, i) was in the extracellular side and forming between the TM1 and TM2 of same monomer (i-i). In the panels A-G all WT and 5-MTSET are represented in black and magenta color respectively. In panels D, E, sets 1,2 and 3 data are represented as circles, crosses and triangles respectively.

We did an extensive hydrogen bond (H-Bond) interaction analysis and discovered that the H-Bond interaction pattern is disturbed by the labels in the MscL channel, particularly backbone-backbone (BB-BB) H-Bonds. The total number of unique BB-BB H-Bonds (a H-Bond in a residue pair type is counted only once) in the WT is greater than in the 5-MTSET ($\approx 5\%$), and this trend is seen in the entire trajectory (Figs. 3 A,B,C). The trend was also

reflected in the transmembrane helices 1 and 2 (TM1 and TM2) of all monomers, except for TM1's of S3 and S5 and TM2 of S4 (Figs. 3 D,E). We hypothesize that the loss of BB-BB H-Bonds in the engineered proteins is believed to make the helices more flexible, which is favorable for the conformational changes that are expected to happen.

Apart from this, we also identified two inter-helical side chain-side chain (SC-SC) H-Bond interactions with significant interaction frequency of WT greater than the 5-MTSET. The first one is N70-N44, which is formed between the TM1 and TM2 of the same monomer (i.e., intra-unit (i-i); each monomer is considered a unit) on the extracellular side (Figs. 3H). The second is D16-Y94, i.e, between the TM1 (D16) of the first and TM2 (Y94) of the preceding monomer (i.e., inter-unit; i-i+4) on the intracellular side (Fig. 3H). The average interaction frequency of N70-N44 in the WT is $\approx 50, 40, 52\%$, and that of the 5-MTSET is $\approx 20, 22, 39\%$ for sets 1, 2 and 3 respectively (Fig. 3F). Where as that of the D16-Y94 in WT and 5-MTSET are 49, 49, 40% and 10, 21, and 19% respectively (Fig. 3G). The N70-N44 interaction might play a key role in keeping the TM1 and TM2 of the monomer intact on the extracellular side and breaking of this interaction might be crucial for the channel to open, which is also reflected in our analysis. The breaking of D16-Y94 interaction in 5-MTSET probably facilitates the formation of R11-E104 (i, i+1) and E7-R98 (i, i+2) salt bridges, which are discussed in more detail in the following section.

**Labels facilitated rearrangement of salt bridge interactions**

Apart from the H-Bond interaction analysis, we also performed the salt bridge interaction analysis. For the purpose of this analysis, instead of considering the entire trajectory, we performed the analysis on trajectories ranging from 300-500ns and 800-1000ns respectively (called A and B in Tables 3, 4). We identified 8 interesting salt bridge interactions and we classified them into 4 different classes as TM1(i)-TM2(i+1), TM1(i)-TM2(i+2), TM2(i)-TM2(i), and TM1(i)-ECL(i+1) for the sake of comparison. We further classify TM1(i)-TM2(i+1), TM1(i)-TM2(i+2), and TM1(i)-ECL(i+1) classes of SB interactions as inter-

**Table 3: Inter-unit salt bridge interaction.**

| SB Class | SB | WT | | 5-MTSET | |
|---|---|---|---|---|---|
| | | A | B | A | B |
| TM1(i)-TM2(i+1) | R11-E104(SB1) | 1/2/1 | 0 | 2/2/2 | 2 |
| TM1(i)-TM2(i+2) | E7-R98(SB2) | 0/0/0 | 0 | 1/1/1 | 1 |
| | R11-D108(SB3) | 2/2/2 | 2 | 3/1/1 | 1 |
| | E7-K99(SB4) | 1/2/3 | 2 | 1/1/0 | 1 |
| TM1(i)-ECL(i+1) | K33-D68(SB5) | 1/0/0 | 0 | 1/1/1 | 1 |
| | D36-R58(SB6) | 0/0/0 | 0 | 0/1/1 | 1 |
| | R45-D53(SB7) | 2/1/1 | 2 | 0/0/0 | 0 |
| Total | | 7/7/7 | 6 | 8/7/6 | 7 |

A and B refers to 300-500ns and 800-1000ns trajectories respectively. Salt bridge interactions with contact frequency $\geq 70\%$ (i.e., the distance between interacting residues was $\leq 4\mathring{A}$ for $\geq 70\%$ of simulation time) were considered. ECL refers to the extracellular loops.

unit SB interactions (i.e., the SB interactions that are occurring between the neighboring monomers/units, Table 3), and the TM2(i)-TM2(i) SB interactions as intra-unit SB interactions (i.e., the SB interactions that are occurring within the same monomer/unit Table 4). Of the 8, 7 are inter-unit SB's and one is a intra-unit SB. The dominating inter-unit interactions in the WT belongs to the class TM1(i)-TM2(i+2), followed by TM1(i)-ECL(i+1) and TM1(i)-TM2(i+1). There is no significant difference in the total number inter-unit SBs between A and B in the WT (7 vs. 6; Table 3). In the case of 5-MTSET, again the dominating interunit SBs are again TM1(i)-TM2(i+2); followed by the classes TM1(i)-ECL(i+1) and TM1(i)-TM2(i+1), which has equal contribution. There is no significant difference between A and B with respect to the total number of SBs in 5-MTSET as well similar to WT (8/7/6 vs. 7; Table 3). Also, there is no significant difference in the total no. of inter-unit SBs between WT and 5-MTSET, both in terms of A and B. However, there is a difference in distribution of these SBs between the WT and 5-MTSET. For example, the # of SBs belonging to the class TM1(i)-TM2(i+1) in WT is 0, where as in 5-MTSET it is 2 (comparing just B in either case). There is only one SB belonging to this class (R11-E104; we call it SB1) and it is on the intracellular side near the bottle neck region (Fig. 4A). Probably the labels facilitated

the formation of these SB1 SBs in the 5-MTSET (total 2). Hence, we believe that the SB1 interactions play a key role in the opening of the channel pore. On average, there is loss of one SB belonging to the TM1(i)-TM2(i+2) in 5-MTSET compared to the WT (4 vs. 3; again comparing B in both cases). There is a loss of one SB3, one SB4, and gain of one SB2 in the 5-MTSET (all 3 belonging to TM1(i)-TM2(i+2) class). SB2 does not exist in the WT at all. With respect to the TM1(i)-ECL(i+1) class, both the WT and 5-MTSET has two SBs each. However, the distribution is different in both cases; WT has only SB7 (R45-D53) belonging to this class, which is completely absent in the 5-MTSET (2 vs. 0). There is a gain of one SB5 and one SB6 in the case of 5-MTSET, which are completely absent in the WT. We believe the difference in the distribution of TM1(i)-ECL(i+1) class of SBs between the WT and 5-MTSET is key for the complete opening of the MscL channel pore. Particularly, SB7 interaction ties the neighboring monomers/units on the extracellular side. Hence the loss of this interaction on the extracellular side is key for the opening of the channel. It is this SB7 interaction that keeps the loops in the outer circumference. In the WT, there are 2 of them keeping the channel intact, where as these interactions are lost (total 0) in the 5-MTSET setting the loops free to move thereby facilitating the loops to collapse into the center of the protein. On the other had, the SB5 and SB6 interactions that are formed in the 5-MTSET (completely absent in WT) on the extracellular side facilitates the loops collapsing into the center of the protein. We hypothesize that the sudden jerk like motion induced by the labels at the bottle neck region facilitates the complete loss of SB7 in 5-MTSET, which in turn facilitates the formation of SBs 5,6 (Fig. 4D). We believe the SBs 5,6 are blocking the complete opening of the engineered MscL channel on the extracellular side. Hence the loss of these 2 SBs (5 and 6) is very important, which did not happen in the limited unbiased MD simulation of ours. Overall, we believe that the gain of two (TM1(i)-TM2(i+1) and loss of one (TM1(i)-TM2(i+2) SB interactions facilitated the opening of the channel on the intracellular side; and gain of SB5 and SB6 on the extracellular side prevented the opening on the extracellular side.

On the other hand, there is a loss of one intra-unit SB interaction (SB8) (Fig. 4B) belonging to the class TM2(i)-TM2(i) in 5-MTSET (2 vs. 1; Table 4). Probably the loss of this particular interaction in 5-MTSET, which is at the intersection of TM helices and the intracellular helices (IH), might make the TM helices and the corresponding IHs more flexible allowing the opening of the channel.

**Table 4: Intra-unit salt bridge interactions.**

| **SB Class** | **SB** | **WT** | | **5-MTSET** | |
|---|---|---|---|---|---|
| | | **A** | **B** | **A** | **B** |
| TM2(i)-TM2(i) | D108-R98(SB8) | 0/1/1 | 2 | 0/0/0 | 1 |
| Total | | 0/1/1 | 2 | 0/0/0 | 1 |

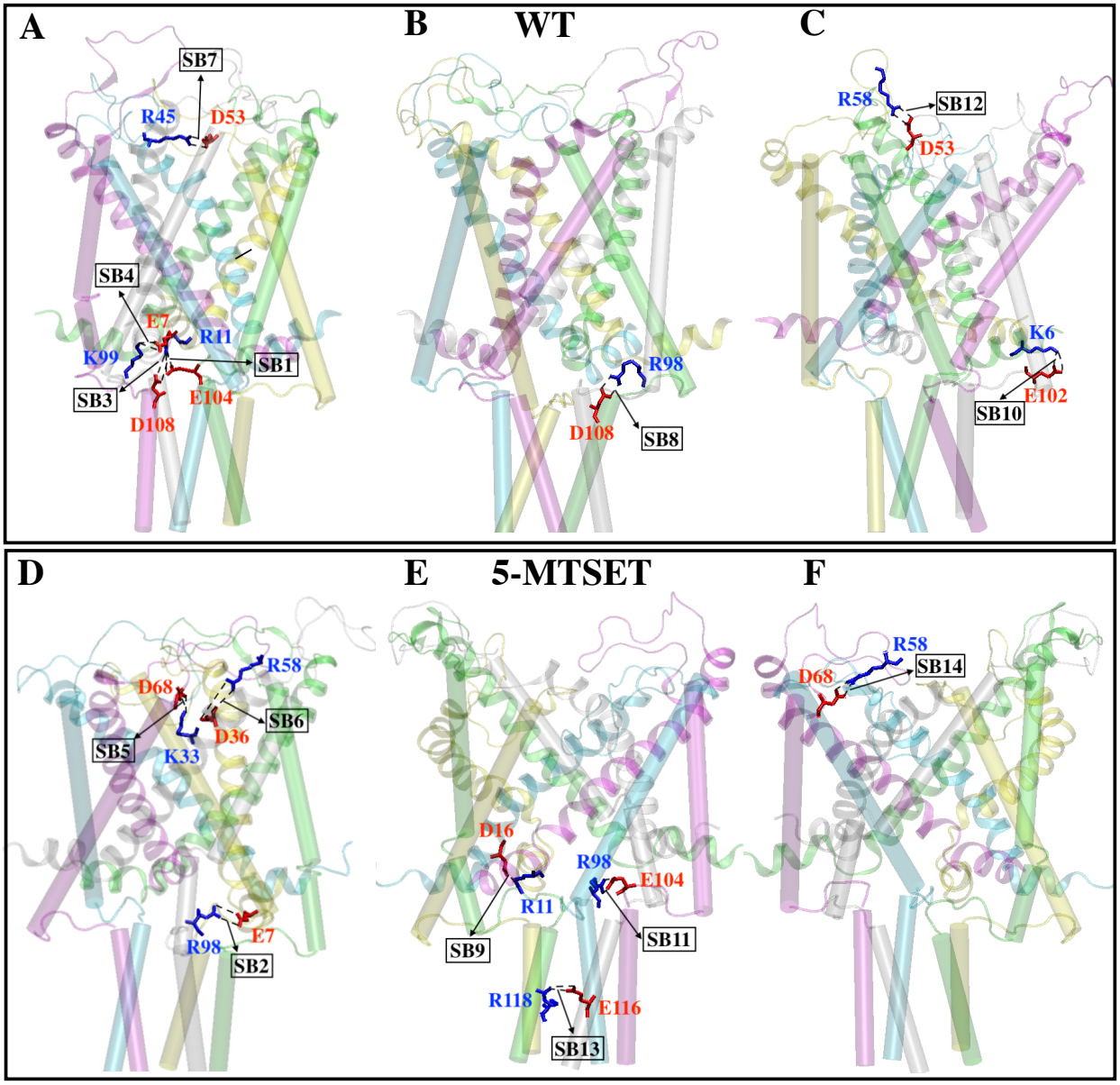


**Fig. 4.** Salt bridge interactions that are playing a key role in the function of engineered MscL channel.

**Orientation angle calculations confirms that the engineered MscL channel opened only partially in equilibration simulations**

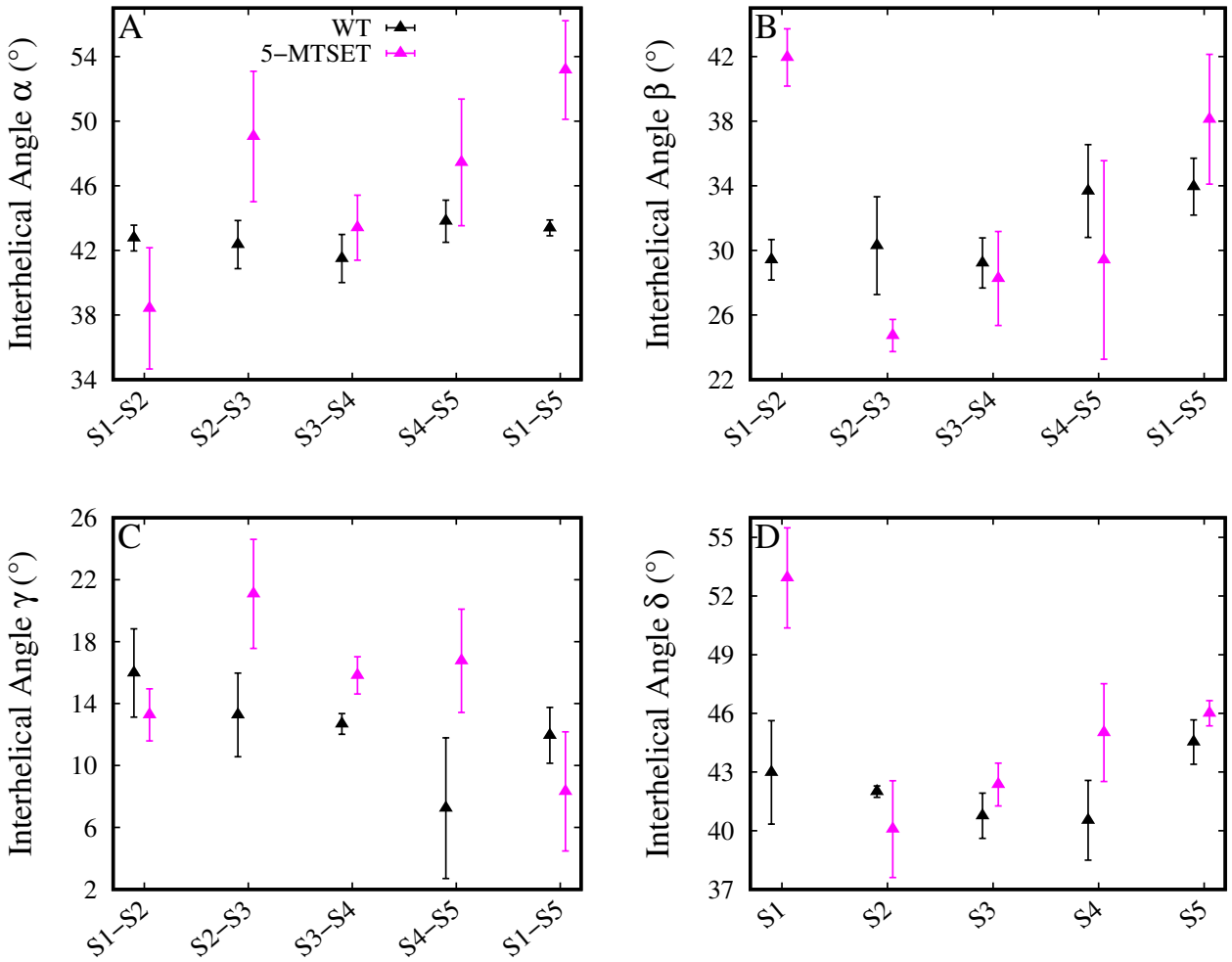


**Fig. 5.** Orientation angles $\alpha$, $\beta$, $\gamma$, and $\delta$. (A-D) Comparing the inter-helical angles $\alpha$ (A), $\beta$ (B), $\gamma$ (C) and $\delta$ (D) between the WT and the 5-MTSET respectively. WT and 5-MTSET data points are represented as black and magenta triangles respectively. Each data point represents the average and standard deviation of all three simulation sets in each case. Only last 300ns of trajectory data is considered for this analysis.

To understand the mechanism of opening of the channel in response to the introduction of positive labels we measured various interhelical angles, which are defined them as $\alpha$, $\beta$ and $\gamma$ and $\delta$ (Fig. 1B). The overall behavior of all 5 angles in each case in WT is very uniform, except in very few limited cases, for example S4-S5 $\gamma$. However, such is not the case with 5-MTSET. The five individual angles in all each case of 5-MTSET are very disperse

and more deviating compared to the WT. Although there is a significant difference in few cases between the WT and 5-MTSET, such as S2-S3 $\alpha$(Fig. 5A), S2-S3 $\beta$(Fig. 5B), S2-S3 $\gamma$(Fig. 5C), S1 $\delta$(Fig. 5D), overall we did not observe a conclusive behavior with respect to 5-MTSET in any of the 4 inter-helical angles. This behavior probably is due to the fact that 5-MTSET is not completely open in the equilibrium simulations.

**Principle Component Analysis (PCA) confirm that loops play a key role in the dynamics of MscL protein**

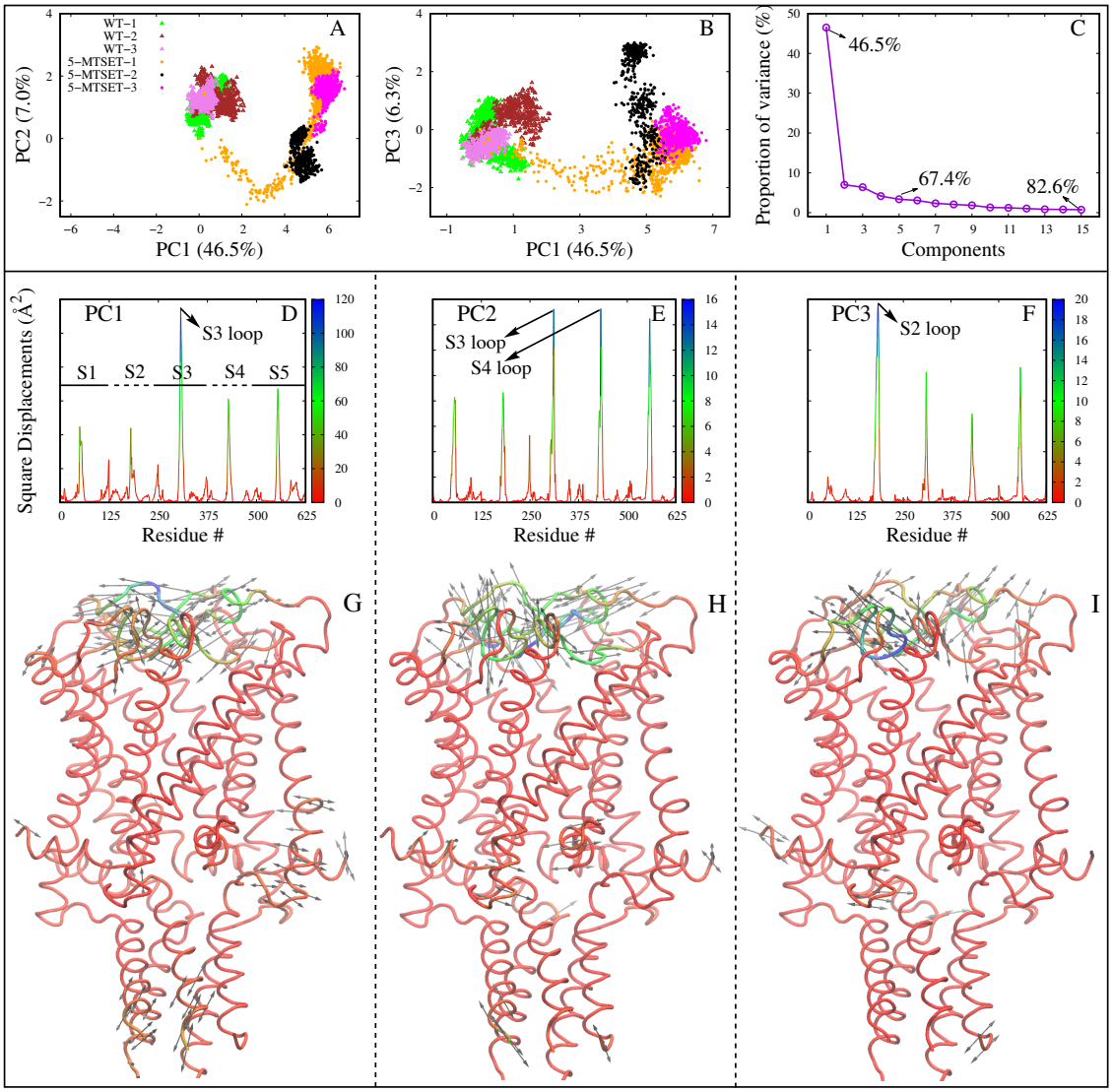


**Fig. 6.** Projections along PC's 1, 2 and 3. (A) PC1 vs. PC2. (B) PC1 vs. PC3. (C) is the proportion of variance (or total mean square displacement) of first 15 principle components. (D-F) Contribution of individual residues (represented as mean square fluctuations of the atom positions) for PCs 1, 2 and 3 respectively. (G-I) Structural variations along PCs 1, 2 and 3 respectively. Structures are colored based on the extent of mobility/fluctuation. Bidirectional arrow shows the direction of the fluctuation of the structure and the length of the arrow reflects the magnitude of fluctuation.

To unveil the principle variations between the WT and engineered structures we performed PCA analysis. Usually the top ranking modes reflect the dominant features responsible for

the variations in the structures. Projections onto principle components PC1 and PC2 clearly discriminates WT, 1-MTSET and 5-MTSET systems (Fig. 6A). The contribution of these two PC's to the total variance is 51.4%. Top 5 PC's contribution to the variance is 64.3% and the top 15 PC's is 81.4%(Fig. 6D). Although, the deviation of the engineered systems from the WT is not huge, all three systems are clustered differently along PC1 space. 5-MTSET systems deviated more than the 1-MTSET systems from the WT. All the triplicate simulations of each system clustered very close to each other, elucidating the fact that the structural variations along PC's 1 and 2 are reproducible and significant. PC2 separates 1-MTSET from 5-MTSET and WT systems (Fig. 6A); PC3 and PC4 shows how dispersed the 5-MTSET system compared to the WT and 1-MTSET systems (Fig. 6B & C).

The structural variation along PC1 is dominated by the loops in S3 monomer (blue colored peak in Fig. 6A) followed by the loops in S4 and S5 monomers (orange and yellow peaks in Fig. 6A). The residue with the highest fluctuation in PC1 is R58 belonging to loop S3 ($\beta = 78.6\mathring{A}$). R58 is involved in salt bridge interactions with D36 and D68 as demonstrated earlier. And the pca analysis supports the earlier salt bridge interaction analysis and supports the hypothesis that the loops are playing a key role in the dynamics and function of MscL channel. After loops the intracellular helices are dominating the fluctuations, especially in the S1 and S2. In the PC2, S1 loop dominates (purple peak in Fig. 6B, residues 50-56) followed by S5 loop (yellow peak in Fig. 6B, residues 56-60). In PC3, again loops dominates and the contribution of all loops is approximately similar Fig. 6C. Followed by loops is the intracellular helix of the S2.

## Trapping the open MscL structure via non-equilibrium and follow-up equilibrium simulations

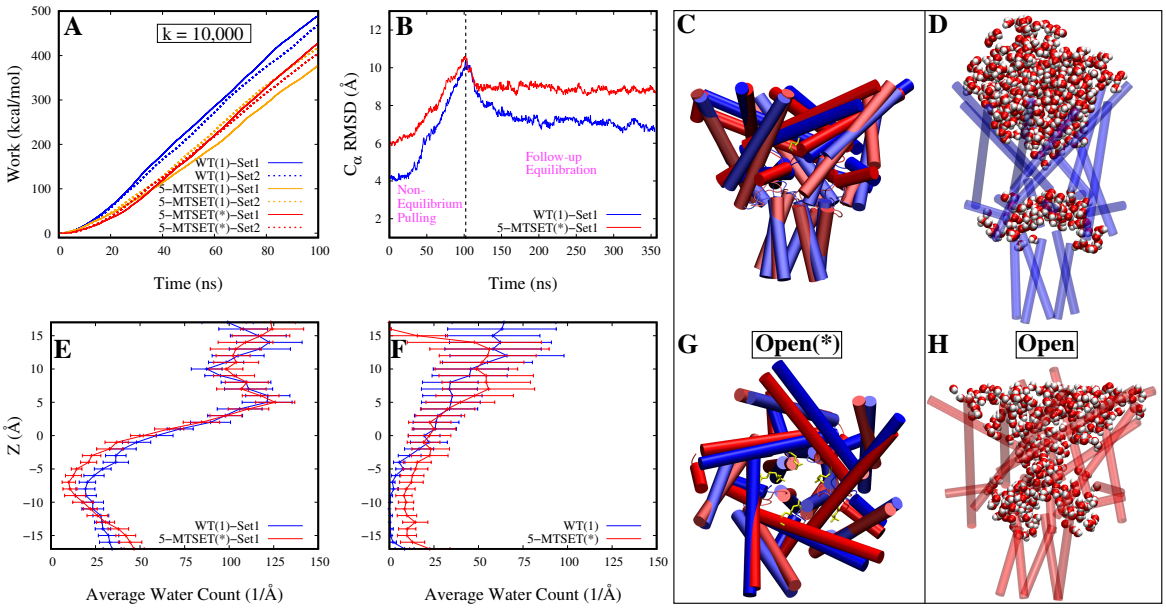


**Fig. 7.** Non-equilibrium and follow-up equilibrium resulted in an open MscL structure. (A) Comparison of WT vs. Engineered MscL (5-MTSET and 5-MTSET(*)) work values as a function of time. (B) protein C$\alpha$ RMSD vs. time during the 100ns non-equilibrium pulling simulation and the follow-up 250ns equilibrium relaxation simulation of WT(1) and 5-MTSET(*) systems. For calculating the C$\alpha$ RMSD of the protein we used crystal structure as reference. (E-F) water count across the pore resulting from 100ns non-equilibrium simulations for WT(1) and 5-MTSET(*) systems, and F is water across the pore during the 250ns follow-up equilibrium simulations. Last 2.5ns simulation was used for the water content calculation. (C) is superposition of open(*) structures of WT(1) and 5-MTSET(*) resulting from non-equilibrium simulations. WT(1) and 5-MTSET(*) are represented in blue and red colors respectively. (G) Same is C except that C is side view and G is the top view. (D,H) Open structures of WT(1) and 5-MTSET(*) structures resulting from follow-up equilibrium simulations. Water within the 3Åof the protein is shown both cases.

Since the unbiased equilibration simulations failed to open either the WT or the engineered MscL structures as explained earlier we conducted non-equilibrium (NE) pulling simulations to force open the resulting unbiased equilibration simulation structures. We have used the SM-FRET based WT active/open structure of MscL as a reference to open these structures.

Orientation collective variables (colvars) module of NAMD was used to direct these structures towards the target. Using this procedure we opened the WT, 5-MTSET and 5-MTSET(*) structures. In each case we repeated the NE pulling simulations to check the reproducibility and each pulling simulation was 100ns long. We compared the work required to open these different structures in NE simulations and WT requires more work to open compared to the 5-MTSET and 5-MTSET(*) structure(Fig. 7A) and this behavior is reproducible. However, we did not see the difference in work values between the 5-MTSET and 5-MTSET(*) structures, which guides us to conclude that there is no impact of the starting orientations of the labels on the opening/activation of the channels. The NE work relations support earlier observations that labels facilitate the opening of the channel. Since these structures were force opened, irrespective of the presence or absence of labels all the structures were opened to the same extent (Fig. 7C), which is reflected in the RMSD calculations (Fig. 7B). Although there is a difference in RMSD between the WT(1) and the 5-MTSET(*) set-1 simulations at the start, by the end of 100ns NE simulation there is no significant difference. However, the extent of opening of the pore near the bottle neck region (z= -5 to -10; the structure sort of flattened while opening, hence the bottle neck region went slightly up compared to the equilibrium simulations) is greater in WT(1) compared to the 5-MTSET(*). This is evident from the water content calculations, where WT(1) has more water in the pore region than the 5-MTSET(*)(7 vs. 22 near the narrowest part of the pore, which is Z = -7 Å)(Fig. 7E). We believe this is because the labels which are predominantly oriented parallel to the membrane normal in the earlier equilibration simulations (Fig. S1B), however, in the NE simulations they are most likely oriented perpendicular to the membrane normal(Fig. 7G), and hence blocking the pore.

To further check the stability of the non-equilibrium structures, we relaxed the set-1 of WT and 5-MTSET(*) non-equilibrium structures via the unbiased equilibration simulations using the protocol explained in Table 2. In these follow-up equilibration simulations both the WT and 5-MTSET(*) structures were not stable, WT collapsed back to the original

state while the 5-MTSET(*) collapsed to a state which is more open than the equilibrated structures (we call it open) (Figs. 7D, H). This also lead us to hypothesize that probably the open/active state of MscL is not as open as the everyone else have thought. This is reflected in the water content calculations, where the average water in the pore in WT is 0 near the bottle neck region and in the 5-MTSET(*) it is $\approx 10$ (Fig. 7F). The water content correlate well with the C$\alpha$ RMSD (Fig. 7B).

## Characterizing the open MscL structures resulting from the follow-up NE simulations

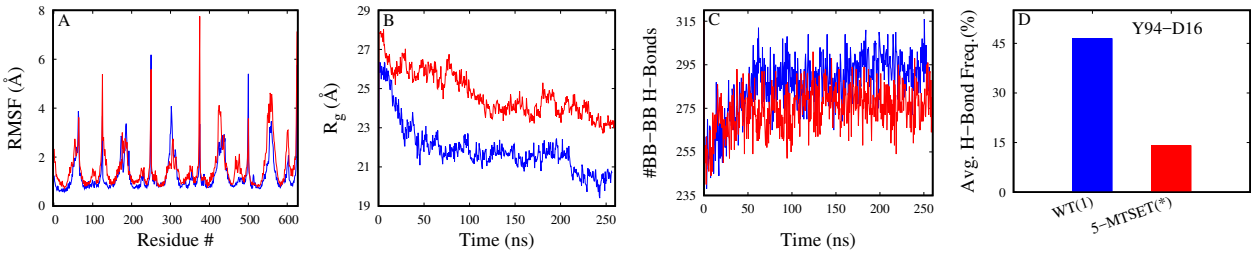


**Fig. 8.** Characterizing the open MscL structure. (A-D) Comparison RMSF (A), Radius of gyration (B), # of BB-BB H-Bonds (C), Avg. Y94-D16 H-Bond frequency (D) between WT(1) vs. 5MTSET(*) systems respectively. WT(1) and 5MTSET(*) data are represented in blue and red respectively. The entire 260ns of follow-up NE simulations data is considered for this calculation.

We further characterized the open WT(1) and 5-MTSET(*) MscL structure resulting from the follow-up NE simulations. We calculated several variables including RMSF, ECL $R_g$, # of BB-BB H-Bonds, Avg. Y94-D16 H-Bond frequency, SC-SC (both inter-/intra-unit) salt bridge interactions and various interhelical angles to compare and contrast between the WT(1) and 5-MTSET(*) open structures. Significant differences between the open WT(1) and 5MTSET(*) open structures were observed. The overall fluctuation of the 5-MTSET(*) structure is greater than the WT(1) (Fig. 8A). The $R_g$ of ECL of both the structures reduced for the entire length of the trajectory. However, the $R_g$ of the 5-MTSET(*) is significantly greater than the WT(1) (Fig. 8b); there is at least 4 Å difference between the two at the

end of the 260ns follow-up NE simulation, which shows that the ECL region of 5-MTSET(*) is more open compared to the WT(1). This is in contrast to the equilibration simulations, where the $R_g$ of the 5-MTSET structures are lower than the WT(Figs. S3 D,F). We would believe this is due to the formation of SBs 5&6 in the equilibrated 5-MTSET structures (Table 3) as explained earlier and we do not see these SBs existing in the 5-MTSET(*) structure in the follow-up NE simulations (Table 5). Similar to the equilibrium simulations the # of BB-BB H-Bonds in 5-MTSET(*) is greater (on average 15) than in the WT(1); although they are similar at the start of the simulations, as the simulations proceeded the difference is significant (Fig. 8C). This establishes the fact that the loss of BB-BB H-Bonds makes the structure more flexible there by facilitating the opening/activation. However, this trend is not clearly visible in the TM region. For example, the # of TM1 BB-BB H-Bonds of S1, S2, and S3 in WT(1) are greater than 5-MTSET(*), where it is opposite for S4 and S5 (Fig. S4E). On the other hand, the # of TM2 BB-BB H-Bonds of S1 and S2 in 5-MTSET(*) are greater than WT(1), where it is opposite for S3, S4 and S5 (Fig. S4F). Also, there is a loss of SC-SC Y94-D16 H-Bond in 5-MTSET(*) ($\approx$ 15 frequency%) compared to the WT(1) ($\approx$ 45% frequency); this behavior is similar to the equilibrium simulations(Fig. 8D). This supports the hypothesis that the loss of this particular H-Bond is key for the activation of engineered MscL channel.

Apart from this, we also calculated the SC-SC SB interactions (both inter-/intra-unit). Unlike the earlier equilibrium simulations, the total # of inter-unit SBs in the case of 5-MTSET(*) is 4 (i.e., the SBs with $\geq$ 70% interaction frequency), where as in the case of WT(1) they are 14. Overall, 5-MTSET(*) has to loose 10 inter-unit SBs compared to the WT)(1) for it to open in the follow-up NE simulations. These 14 inter-unit SBs identified in the WT(1) is classified into 7 different classes as shown in Table 5. Of the 7, two were already introduced earlier (TM1(i)-TM2(i+2) and TM1(i)-ECL(i+1); Table 3) and 5 were introduced here since these classes of SBs were not found earlier in the equilibrium simulations in either WT or 5-MTSET structures. The 14 WT(1) SBs are spread all over the channel, however, the

dominating interactions are between the TM1 and TM2 of the neighbor units (total 6 of 14). It is very interesting that we found 14 in WT(1) in the follow-up NE simulations, where as we identified only 6 in the earlier equilibration simulations. This is probably because the gain of 8 new SBs in the WT(1) is needed for the WT(1) protein to collapse back to the original state. Where as in the case of 5-MTSET(*) there is a overall loss of ≈ 3 SBs compared to the 5-MTSET in the earlier equilibration simulations (≈4 vs. ≈7). The two classes of SBs that were observed in the 5-MTSET in the equilibrium simulations, i.e., TM1(i)-TM2(i+1) and TM1(i)-ECL(i+1), are completely lost in the NE follow-up equilibrium simulations. This supports our earlier hypothesis that the loss of TM1(i)-ECL(i+1) SBs are key for the complete opening of the engineered channel. There is not a single SB involving ECL in the case of 5-MTSET(*), which further supports our hypothesis. However, there is gain of 3 new classes of SBs in 5-MTSET(*) in NE follow-up equilibrium simulations, TM1(i)-TM1(i+1), TM2(i)-TM2(i+1), and IH(i)-IH(i+1). Also, there is a gain of 2 new intra-unit SBs in 5-MTSET(*) (Table 6) and these two belong to the class ECL(i)-ECL(i) (again this is a new class that was not found in the earlier equilibrium simulations). These two were not also observed in the WT(1).

**Table 5: Inter-unit salt bridge interaction.**

| SB Class | SB | WT(1) | 5-MTSET(*) |
|---|---|---|---|
| TM1(i)-TM2(i+2) | R11-D108(SB3) | 2 | 1 |
| | E7-K99(SB4) | 1 | 0 |
| TM1(i)-ECL(i+1) | R45-D53(SB7) | 1 | 0 |
| TM1(i)-TM1(i+1) | R11-D16(SB9) | 2 | 1 |
| TM1(i)-TM2(i+1) | K6-E102(SB10) | 3 | 0 |
| TM2(i)-TM2(i+1) | R98-E104(SB11) | 2 | 1 |
| ECL(i)-ECL(i+1) | D53-R58(SB12) | 1 | 0 |
| IH(i)-IH(i+1) | E116-R118(SB13) | 2 | 1 |
| **Total** | | 14 | 4 |

Only last 100ns of relaxation simulation trajectory is considered. IH refers to intracellular helices. Interactions with >70% are considered. SB is salt bridge.

**Table 6: Intra-unit salt bridge interaction.**

| SB Class | SB | WT(1) | 5-MTSET(*) |
|---|---|---|---|
| ECL(i)-ECL(i) | D68-R58(SB14) | 0 | 2 |
| **Total** | | 0 | 2 |

Only last 100ns of relaxation simulation trajectory is considered.

## Proposed mechanism of action

Based on our detailed analysis of the equilibrium, non-equilibrium and follow-up equilibration simulation data we propose a hypothesis for the opening/activation of the engineered MscL channel. According to the hypothesis, first the channel opens spontaneously due to the repulsion between engineered positively charged labels and also due to steric clashes between the labels and other bottle neck residues, which is also demonstrated through interaction analysis (8 among the top 10 residues interacting with the labels are non-polar ( Table S1)). This sudden jerk like motion near the bottle neck region lead to the breaking of inter-unit SB7 interaction (TM1(i)-ECL(i+1)) on the extracellular side, which let the loops free and collapse to the center of the protein (depicted by the reduction of radius of gyration ($R_g$))(Figs. S3 C,D), which in-turn is facilitated by the forming of the inter-unit salt bridge interactions SB5 and SB6 (TM1(i)-ECL(i+1)) interactions on the extracellular side. We believe that the salt bridge interactions SB5 and SB6 (TM1(i)-ECL(i+1)) is resisting the opening of the channel on the extracellular side and breaking of these interactions is key for the opening of the protein on the extracellular side completely. Subsequent loss of SB5 and SB6 interactions leads to the opening of the channel completely, which is facilitated by breaking of several classes of inter-unit salt bridge interactions spread all over the channel ($\approx$ 10 as shown in Table 5) and an inter-unit hydrogen bond (Y94-D16) facilitating the opening of the channel. This is also facilitated by the loss of BB-BB H-Bonds, loosening the TM helices ((Fig. 8D)). Further, the non-polar amino acids L17 and A18 that sits between the labels on the intracellular side are reducing the repulsion between the positively charged labels and are restricting the extent of the opening of the channel.

# Conclusions

In this study we performed all-atom un-biased equilibrium and non-equilibrium MD simulations of the wild-type and the engineered MscL channels to study the mechanism of opening of the channel in atomistic detail for the first time. In the equilibrium MD simulations, we identified that the labels facilitated opening of the engineered MscL channel, although not completely, which may be due to the time scale associated with the opening of the channel. Opening of the channel started near the labels and the salt bridge interactions between the extracellular loops and the TM helices are restricting the opening of the channel on the extracellular side, there by restricting the complete opening of the channel. Therefore, we utilized non-equilibrium simulations followed by the relaxation of the resulting non-equilibrium structures via un-biased MD simulations, which resulted in an open/active conformation of the engineered MscL channel. The open/active conformation we captured is not as open as it has been proposed earlier. Overall, according to the mechanism we proposed here for the activation of this engineered channel, the ECL loops are playing a key role in the opening of the engineered channel. Also, the loss of several BB-BB H-Bonds and several SC-SC salt bridge interactions facilitate the opening of the channel.

# Acknowledgement

This research is supported by the University of Arkansas, Fayetteville. This research is part of the Blue Waters sustained-petascale computing project, which is supported by the National Science Foundation (awards OCI-0725070 and ACI-1238993) and the state of Illinois. Blue Waters is a joint effort of the University of Illinois at Urbana-Champaign and its National Center for Supercomputing Applications. This research is also supported by the Arkansas High Performance Computing Center which is funded through multiple National Science Foundation grants and the Arkansas Economic Development Commission.

## Supporting Information Available

Figures S1–S4 and Tables S1-S2 in Supporting Information provide additional analysis based on our MD trajectories as discussed in the manuscript.

## References


(1) Sukharev, S. I.; Blount, P.; Martinac, B.; Kung, C. Mechanosensitive Channels of Escherichia Coli: The MscL Gene, Protein, and Activities. *Annu. Rev. Physiol.* **1997**, *59*, 633 – 657.

(2) Kocer, A. Mechanisms of mechanosensing  mechanosensitive channels, function and re-engineering. *Current Opinion in Chemical Biology* **2015**, *29*, 120 – 127.

(3) Moe, P. C.; Levin, G.; Blount, P. Correlating a Protein Structure with Function of a Bacterial Mechanosensitive Channel. *J. Biol. Chem.* **2000**, *275*, 31121 – 31127.

(4) Moe, P.; Blount, P. Assessment of Potential Stimuli for Mechano-Dependent Gating of MscL: Effects of Pressure, Tension, and Lipid Headgroups. *Biochemistry* **2005**, *44*, 12239 – 12244.

(5) Markin, V. S.; Martinac, B. Mechanosensitive ion channels as reporters of bilayer expansion. A theoretical model. *Biophys. J.* **1991**, *60*, 1120 – 1127.

(6) Perozo, E.; Kloda, A.; Cortes, D. M.; Martinac, B. Physical principles underlying the transduction of bilayer deformation forces during mechanosensitive channel gating. *Nat. Struct. Biol.* **2002**, *9*, 696–703.

(7) Yoshimura, K.; Batiza, A.; Kung, C. Chemically charging the pore constriction opens the mechanosensitive channel MscL. *Biophys. J.* **2001**, *80*, 2198 – 2206.

(8) Kocer, A.; Walko, M.; Bulten, E.; Helza, E.; Feringa, B. L.; Mieijberg, W. Rationally Designed Chemical Modulators Convert a Bacterial Channel Protein into a pH-Sensory Valve. *Angewandte Chemie International Edition* **2006**, *45*, 3126 – 3130.

(9) Kocer, A. A Remote Controlled Valve in Liposomes for Triggered Liposomal Release. *Journal of Liposome Research* **2007**, *17*, 219–225.

(10) van den Bogaart, G.; Krasnikov, V.; Poolman, B. Dual-color fluorescence-burst analysis to probe protein efflux through the mechanosensitive channel MscL. *Biophys. J.* **2007**, *92*, 1233 – 1240.

(11) Powl, A. M.; East, J. M.; ; Lee, A. G. Anionic phospholipids affect the rate and extent of flux through the mechanosensitive channel of large conductance MscL. *Biochemistry* **2008**, *47*, 4317 – 4328.

(12) Price, C. E.; Kocer, A. K. A.; Kol, S.; van der Berg, J. P.; Driessen, A. J. M. In vitro synthesis and oligomerization of the mechanosensitive channel of large conductance, MscL, into a functional ion channel. *FEBS Letters* **2011**, *585*, 249 – 254.

(13) Birkner, J. P.; Poolman, B.; Kocer, A. Hydrophobic gating of mechanosensitive channel of large conductance evidenced by single-subunit resolution. *Proc. Natl. Acad. Sci. USA* **2012**, *109*, 12944 – 12949.

(14) Iscla, I.; Eaton, C.; Parker, J.; Wray, R.; Kovcs, Z.; Blount, P. Improving the Design of a MscL-Based Triggered Nanovalve. *Biosensors* **2013**, *3*, 171.

(15) Pacheco-Torres, J.; Mukherjee, N.; Walko, M.; Lpez-Larrubia, P.; Ballesteros, P.; Cerdan, S.; Kocer, A. Image guided drug release from pH-sensitive Ion channel-functionalized stealth liposomes into an in vivo glioblastoma model. *Nanomedicine: Nanotechnology, Biology and Medicine* **2015**, *11*, 1345 – 1354.

(16) Louhivuori, M.; Risselada, H. J.; van der Giessen, E.; Marrink, S. J. Release of content through mechano-sensitive gates in pressurized liposomes. *Proceedings of the National Academy of Sciences* **2010**, *107*, 19856–19860.

(17) Deplazes, E.; Louhivuori, M.; Jayatilaka, D.; Marrink, S. J.; Corry, B. Structural Investigation of MscL Gating Using Experimental Data and Coarse Grained MD Simulations. *PLoS Comput. Biol.* **2012**, *8*, e1002683.

(18) Melo, M. N.; Arnarez, C.; Sikkema, H.; Kumar, N.; Walko, M.; Berendsen, H. J.; Kocer, A.; Marrink, S. J.; Ingólfsson, H. I. High-throughput simulations reveal membrane-mediated effects of alcohols on MscL gating. *Journal of the American Chemical Society* **2017**,

(19) Gullingsrud, J.; Kosztin, D.; Schulten, K. Structural Determinants of MscL Gating Studied by Molecular Dynamics Simulations. *Biophys. J.* **2001**, *80*, 2074–2081.

(20) Gullingsrud, J.; Schulten, K. Gating of MscL Studied by Steered Molecular Dynamics. *Biophys. J.* **2003**, *85*, 2087–2099.

(21) Gullingsrud, J.; Schulten, K. Lipid bilayer pressure profiles and mechanosensitive channel gating. *Biophys. J.* **2004**, *86*, 3496–3509.

(22) Rui, H.; Kumar, R.; ; Im, W. Membrane Tension, Lipid Adaptation, Conformational Changes, and Energetics in MscL Gating. *Biophys. J.* **2011**, *101*, 671 – 679.

(23) Xie, J.-Y.; Ding, G.-H. Studies on sensitivity to tension and gating pathway of MscL by molecular dynamic simulation. *Acta Mechanica Sinica* **2013**, *29*, 256 – 266.

(24) Betanzos, M.; Chiang, C. S.; Guy, H. R.; Sukharev, S. A large iris-like expansion of a mechanosensitive channel protein induced by membrane tension. *Nature Structural Biology* **2002**, *9*, 704 – 710.

(25) Tang, Y.; Cao, G.; Chen, X.; Yoo, J.; Yethiraj, A.; Cui, Q. A Finite Element Framework for Studying the Mechanical Response of Macromolecules: Application to the Gating of the Mechanosensitive Channel MscL. *Biophysical Journal* **2006**, *91*, 1248 – 1263.

(26) Bavi, O.; Vossoughi, M.; Naghdabadi, R.; Jamali, Y. The effect of local bending on gating of MscL using a representative volume element and finite element simulation. *Channels* **2014**, *8*, 344–349.

(27) Pak, O. S.; Young, Y.-N.; Marple, G. R.; Veerapaneni, S.; Stone, H. A. Gating of a mechanosensitive channel due to cellular flows. *Proceedings of the National Academy of Sciences* **2015**, *112*, 9822–9827.

(28) Coutsias, E. A.; Seok, C.; Dill, K. A. Using quaternions to calculate RMSD. *J. Chem. Phys.* **2004**, *25*, 1849–1857.

(29) Horn, B. K. P. Closed-form solution of absolute orientation using unit quaternions. *J. Opt. Soc. Am.Ã* **1987**, *4*, 629–642.

(30) Fiorin, G.; Klein, M. L.; Hénin, J. Using collective variables to drive molecular dynamics simulations. *Mol. Phys.* **2013**, *111*, 3345–3362.

(31) Moradi, M.; Tajkhorshid, E. Mechanistic picture for conformational transition of a membrane transporter at atomic resolution. *Proc. Natl. Acad. Sci. USA* **2013**, *110*, 18916–18921.

(32) Moradi, M.; Enkavi, G.; Tajkhorshid, E. Atomic-level characterization of transport cycle thermodynamics in the glycerol-3-phosphate:phosphate transporter. *Nat. Commun.* **2015**, *6*, 8393.

(33) Steinbacher, S.; Bass, R. B.; Strop, P.; Rees, D. C. In *Current Topics in Membranes in Mechanosensitive Ion Channels, Part A*; Hamill, O. P., Ed.; Elsevier Inc.: New York, NY, 2007; Vol. 58; pp 1–24.

(34) Chemical Computing Group Inc., *Molecular Operating Environment(MOE),2013.08 2016*.

(35) Jo, S.; Kim, T.; Im, W. Automated builder and database of protein/membrane complexes for molecular dynamics simulations. *PLoS One* **2007**, *2*, e880.

(36) Lee, J.; Cheng, X.; Swails, J. M.; Yeom, M. S.; Eastman, P. K.; Lemkul, J. A.; Wei, S.; Buckner, J.; Jeong, J. C.; Qi, Y. et al. CHARMM-GUI input generator for NAMD, GROMACS, AMBER, OpenMM, and CHARMM/OpenMM simulations using the CHARMM36 additive force field. *J. Chem. Theory Comp.* **2016**, *12*, 405–413.

(37) Jorgensen, W. L.; Chandrasekhar, J.; Madura, J. D.; Impey, R. W.; Klein, M. L. Comparison of simple potential functions for simulating liquid water. *J. Chem. Phys.* **1983**, *79*, 926–935.

(38) Phillips, J. C.; Braun, R.; Wang, W.; Gumbart, J.; Tajkhorshid, E.; Villa, E.; Chipot, C.; Skeel, R. D.; Kale, L.; Schulten, K. Scalable molecular dynamics with NAMD. *J. Comp. Chem.* **2005**, *26*, 1781–1802.

(39) Martyna, G. J.; Tobias, D. J.; Klein, M. L. Constant pressure molecular dynamics algorithms. *J. Chem. Phys.* **1994**, *101*, 4177–4189.

(40) Feller, S. E.; Zhang, Y.; Pastor, R. W.; Brooks, B. R. Constant pressure molecular dynamics simulation: The Langevin piston method. *J. Chem. Phys.* **1995**, *103*, 4613–4621.

(41) Klauda, J. B.; Venable, R. M.; Freites, J. A.; O'Connor, J. W.; Tobias, D. J.; Mondragon-Ramirez, C.; Vorobyov, I.; MacKerell Jr., A. D.; Pastor, R. W. Update of the CHARMM all-atom additive force field for lipids: Validation on six lipid types. *J. Phys. Chem. B* **2010**, *114*, 7830–7843.

(42) Best, R. B.; Zhu, X.; Shim, J.; Lopes, P. E. M.; Mittal, J.; Feig, M.; MacKerell, A. D. Optimization of the additive CHARMM all-atom protein force field targeting improved sampling of the backbone $\phi$, $\psi$ and side-chain $\chi 1$ and $\chi 2$ dihedral angles. *J. Chem. Theory Comp.* **2012**, *8*, 3257–3273.

(43) Reid, J. K. In *Large Sparse Sets of Linear Equations*; Reid, J. K., Ed.; Academic Press: London, 1971; pp 231–254.

(44) Darden, T.; York, D.; Pedersen, L. G. Particle mesh Ewald: An $N{\cdot}\log(N)$ method for Ewald sums in large systems. *J. Chem. Phys.* **1993**, *98*, 10089–10092.

(45) Humphrey, W.; Dalke, A.; Schulten, K. VMD: visual molecular dynamics. *J. Mol. Graphics* **1996**, *14*, 33–38.

(46) Bakan, A.; Meireles, L. M.; Bahar, I. ProDy: protein dynamics inferred from theory and experiments. *Bioinformatics* **2011**, *27*, 1575–1577.

(47) Bakan, A.; Bahar, I. The intrinsic dynamics of enzymes plays a dominant role in determining the structural changes induced upon inhibitor binding. *Proc. Natl. Acad. Sci. USA* **2009**, *106*, 14349–14354.

(48) Lange, O. F.; Lakomek, N.-A.; Farès, C.; Schröder, G. F.; Walter, K. F. A.; Becker, S.; Meiler, J.; Grubmüller, H.; Griesinger, C.; de Groot, B. L. Recognition dynamics up to microseconds revealed from an RDC-derived ubiquitin ensemble in solution. *Science* **2008**, *320*, 1471–1475.